

Tang, G.-J., et al., 2023, Large-scale rare-metal pegmatite deposit formation driven by supercontinent assembly: *Geology*, <https://doi.org/10.1130/G51454.1>

## Supplemental Material

**Sample description and data collection and Figures S1–S5.**

**Tables S1–S7.**

**Supporting Information for**  
**Large-scale rare-metal pegmatite deposit formation driven by**  
**supercontinent assembly**

Gong-Jian. Tang<sup>1,2,\*</sup>, Derek. A. Wyman<sup>3</sup>, Qiang. Wang<sup>1,2</sup>, Wei. Dan<sup>1,2</sup>, Lin. Ma<sup>1,2</sup>,  
Ya-Nan. Yang<sup>1,2</sup>

1 State Key Laboratory of Isotope Geochemistry, Guangzhou Institute of Geochemistry,  
Chinese Academy of Sciences, Guangzhou 510640, China

2 CAS Center for Excellence in Deep Earth Science, Guangzhou 510640, China

3 School of Geosciences, Division of Geology and Geophysics, The University of Sydney,  
NSW 2006, Australia

\* Corresponding author, Email: [tanggj@gig.ac.cn](mailto:tanggj@gig.ac.cn) (G.J. Tang)

**Text S1. Sample description and data collection**

In order to evaluate the genetic relationship between the rare-metal pegmatites, barren pegmatites and granitoids in the Bailongshan deposit (Figure S1), we collect different types of samples, including granodiorite, two-mica granite, spodumene-bearing and absent pegmatites. The granodiorite consists of quartz, feldspar, hornblende and biotite. The two-mica granite consists of quartz, feldspar, biotite and muscovite, and minor tourmaline and garnet. Geochemically, the granodiorites are I-type, whereas the two-mica granite are S-type. The Li-poor (spodumene-absent) pegmatite consists of irregular quartz, albite and muscovite. The Li-rich (spodumene-bearing) pegmatite consists of quartz, albite, muscovite, spodumene, and small proportions of montebrasite. The pegmatites exhibit coarse-grained with most grain size is about 1–3 cm. In order to avoid extreme heterogeneity in modal mineralogy for elements analyses, ca. 2.5–3.5 kg of rock has been sampled for each sample.

To better understand the rare metals enrichment processes, we select granitoid samples across the western Kunlun. The granitoids are range from Neo-Proterozoic to Late

Triassic. In addition, the Triassic sedimentary rocks and granulite samples in the western Kunlun were also selected. The granitoids and granulites were selected for elemental analyses. Representative sample descriptions by this study are presented in [Figure S2](#).

Furthermore, we synthesized the published geochronological data ([Table S7](#)) and zircon Hf isotope data ([Table S8](#)) of the rare-metal pegmatites and associated granites, whole-rock elemental data ([Table S8](#)) for magmatic rocks and metasedimentary rocks associated with rare-metal pegmatite deposits from the Altai, western Kunlun and Songpan-Ganze in East Asia.

## **Text S2. Analytical methods**

### ***Zircon separation and preparation***

The zircon grains from granites and pegmatites in the Bailongshan deposit were separated by conventional magnetic and heavy liquid techniques. In order to illustrate zircon internal structures and choose target sites for *in situ* analysis, Cathodoluminescence (CL) images were made using a Carl Zeiss Field Emission Scanning Electron Microscope equipped with Gatan MonnCL4 at the Guangzhou Institute of Geochemistry, Chinese Academy of Sciences (GIG-CAS). [Figure S3A](#) shows the representative zircon CL images.

### ***In situ zircon U-Pb dating and Hf isotope analysis***

Zircon grains from the I- and S-type granites in the Bailongshan deposit were analysed for U, Th and Pb isotopes using a Cameca IMS-1280 HR secondary ion mass spectrometer (SIMS) at GIG-CAS. A primary beam of negative ion  $O_2^-$  with an intensity of about 10 nA was accelerated at high voltage of -13 kV toward the sample surface, yielding an ellipsoidal analysis spot of ca. 20×30  $\mu m$  in size. Measured U/Pb ratios were calibrated against the ~337 Ma zircon U-Pb standard Plešovice ([Sláma et al., 2008](#)) based on an observed linear relationship between  $\ln(^{206}Pb/^{238}U)$  and  $\ln(^{238}U^{16}O_2/^{238}U)$  ([Whitehouse et al., 1997](#)). The data processing procedures were same to those described by [Li et al. \(2010\)](#). Another zircon U-Pb standard Qinghu ([Li et al., 2013](#)) was analyzed along with other unknown zircon samples to serve as the quality control sample. In this study, 11 measurements on zircon standard Qinghu in this study yielded a concordant age of 160.1

$\pm 1.6$  Ma ( $2\sigma$ ), which is within analytical uncertainty of the recommended value of  $160 \pm 3$  Ma (Li et al., 2013).

Zircon U-Pb isotopes for the three samples of S-type granite (14QW143, 14QW145-1 and BLS10) and three samples of pegmatite (BSL41, BLS1746 and BLS1724) in the Bailongshan deposit were analyzed using an Agilent Q-ICPMS equipped with a 193 nm excimer laser ablation system at GIG-CAS. LA-ICPMS analyses were calibrated relative to the zircon standard 91500 (Wiedenbeck et al., 1995) and the standard silicate glass NIST 610 (Jochum et al., 2011), with a beam diameter of 30  $\mu$ m. Zircon standards GJ-1 and Plesovice were analyzed as unknown samples inserted between 91500 and the samples (i.e. two 91500 + one GJ-1 + one Plesovice + Six zircon samples + two 91500) to control the analytical reproducibility.

Time-dependent drifts of U-Th-Pb isotopic ratios were corrected using linear interpolation (with time) for every 10 analyses based on the variations of 91500. The detailed calibration formula and the calculation of standard error have been given by Liu et al. (2010). NIST SRM 610 was used as an external standard for U, Th, and Pb contents calibration. The NIST SRM 610 was analyzed every 10 analyses to correct for the mass discrimination and time-drift of sensitivity for the analyses of U, Th, and Pb. Off-line selection and integration of background and analyte signals, time-drift correction, quantitative calibration for U, Th, and Pb contents, and U-Pb dating were performed using ICPMSDataCal software. The weighted mean  $^{206}\text{Pb}/^{238}\text{U}$  ages for Plešovice and GJ-1 in this study are  $337.9 \pm 2.1$  Ma ( $2\sigma$ ,  $n = 29$ ; MSWD = 0.75) and  $602.5 \pm 2.8$  Ma ( $2\sigma$ ,  $n = 49$ ; MSWD = 1.2), respectively. All these results are in good agreement with the recommended values of Sláma et al. (2008) ( $337.1 \pm 0.4$  Ma,  $2\sigma$ ) for Plešovice and Jackson et al. (2004) ( $600.4 \pm 0.8$  Ma) for GJ-1. The zircon U-Pb data reduction was carried out using Isoplot 4.15 program (Ludwig, 2003). Figure S3B shows the zircon U-Pb Concordia diagrams, and zircon U-Pb age data are presented in Table S2.

Trace element analysis of zircons was conducted by LA-ICP-MS at the Wuhan SampleSolution Analytical Technology Co., Ltd., Wuhan, China. Detailed operating

conditions for the laser ablation system and the ICP-MS instrument and data reduction are the same as description by [Zong et al. \(2017\)](#). Laser sampling was performed using a GeolasPro laser ablation system that consists of a COMPexPro 102 ArF excimer laser (wavelength of 193 nm and maximum energy of 200 mJ) and a MicroLas optical system. An Agilent 7900 ICP-MS instrument was used to acquire ion-signal intensities. Helium was applied as a carrier gas. Argon was used as the make-up gas and mixed with the carrier gas via a T-connector before entering the ICP. A “wire” signal smoothing device is included in this laser ablation system ([Hu et al., 2015](#)). The spot size and frequency of the laser were set to 32  $\mu\text{m}$  and 6 Hz, respectively, in this study. Trace element compositions of minerals were calibrated against various reference materials (BHVO-2G, BCR-2G and BIR-1G) without using an internal standard ([Liu et al., 2008](#)). Each analysis incorporated a background acquisition of approximately 20-30 s followed by 50 s of data acquisition from the sample. An Excel-based software ICPMSDataCal was used to perform off-line selection and integration of background and analyzed signals, time-drift correction and quantitative calibration for trace element analysis ([Liu et al., 2008](#)). Analytical precisions for most elements are better than 20%. Detailed zircon trace element data are given in [Table S3](#).

*In situ* zircon Hf isotopes were measured using a Geolas-193 laser-ablation system connected to a Thermo Neptune Plus multi-collector ICP-MS at GIG-CAS. The detail analytical procedures were similar to those described by [Wu et al. \(2006\)](#). The analyses for the U-Pb age and Hf isotopes were conducted on the same cathodoluminescence domains. The Hf isotope analyses were conducted with beam diameters of 44  $\mu\text{m}$ , 10 Hz repetition rates, laser beam energy density of 10 J/cm<sup>2</sup>, and 26 seconds of ablation time. In order to evaluate the data accuracy and precision, zircon 91500 was used as an external standard for correcting mass discrimination and time-drift (Blichert-Toft, 2008). Zircon standard Plesovice ([Sláma et al., 2008](#)) and GJ-1 ([Morel et al., 2008](#)) were analyzed as unknown samples that were regularly measured between zircon 91500 and the samples. The weighted mean <sup>176</sup>Hf/<sup>177</sup>Hf ratios for Plesovice and GJ-1 are  $0.282478 \pm 0.000007$  (2 $\sigma$ , n=48; MSWD =0.22) and  $0.282014 \pm 0.000007$  (2 $\sigma$ , n = 12; MSWD = 0.42), respectively, which are consistent with the recommended values of ([Sláma et al., 2008](#)) ( $0.282482 \pm$

0.000013, 2  $\sigma$ ) and (Morel et al., 2008) ( $0.282000 \pm 0.000005$ , 2  $\sigma$ ). Table S4 shows the *in situ* zircon Hf isotope data.

#### ***In situ apatite Nd isotope analysis***

*In situ* Nd isotope analysis for apatite from the granite and pegmatite in the Bailongshan deposit were analysed using a Neptune Plus MC-ICP-MS equipped with a Geolas HD excimer ArF laser ablation system at the Wuhan Sample Solution Analytical Technology Co., Ltd, Hubei, China. The *in situ* Nd isotope analysis were conducted on with beam diameters ranging from 32 to 90  $\mu\text{m}$  dependent on Nd signal intensity, 4 to 10 Hz pulse frequency at 8 J/cm<sup>2</sup> of laser fluence. The detail analytical procedures were described by Hu et al. (2015). Durango and MAD of two natural apatite megacrysts (Xu et al., 2015) were analysed as unknown samples in order to verify the accuracy of the calibration method. The measured data reduction for the apatite Nd isotope ratios was performed by “Iso-Compass” software (Zhang et al., 2020). Apatite Nd isotope data are presented in Table S5.

#### ***Whole-rock geochemistry and Sr-Nd isotopic analysis***

Whole-rock major and trace elements, and Sr-Nd isotopes analyses for the studied samples, were performed at GIG-CAS.

The sample pretreatment of whole rock major element analysis was made by melting method. The flux is a mixture of lithium tetraborate, lithium metaborate and lithium fluoride (45:10:5), Ammonium nitrate and lithium bromide were used as oxidant and release agent, respectively. The melting temperature was 1050 °C and the melting time was 15min. Major element oxides were analyzed on fused glass beads using a Rigaku RIX 2000 X-ray fluorescence spectrometer, and analytical uncertainties are between 1% and 5%.

Trace elements analyses were conducted on a Perkin–Elmer Sciex ELAN6000 inductively coupled plasma source mass spectrometer (ICP-MS). Analytical precisions for most elements are better than 5%.

Whole-rock Sr and Nd isotopic analyses were performed on a Micromass Isoprobe multicollector ICP-MS, using analytical procedures described by [Li et al. \(2006\)](#). Sr and rare earth elements (REEs) were separated using cation columns, and Nd fractions were further separated with HDEHP-coated Kef columns. Measured  $^{87}\text{Sr}/^{86}\text{Sr}$  and  $^{143}\text{Nd}/^{144}\text{Nd}$  ratios were normalized to  $^{86}\text{Sr}/^{88}\text{Sr} = 0.1194$  and  $^{146}\text{Nd}/^{144}\text{Nd} = 0.7219$ , respectively. The reported  $^{87}\text{Sr}/^{86}\text{Sr}$  and  $^{143}\text{Nd}/^{144}\text{Nd}$  ratios were adjusted to the NBS SRM 987 standard with  $^{87}\text{Sr}/^{86}\text{Sr} = 0.71025$  and the Shin Etsu JNdi-1 standard with  $^{143}\text{Nd}/^{144}\text{Nd} = 0.512115$ . The whole-rock Sr-Nd isotope data are listed in [Table S6](#).

## Supplementary Figures

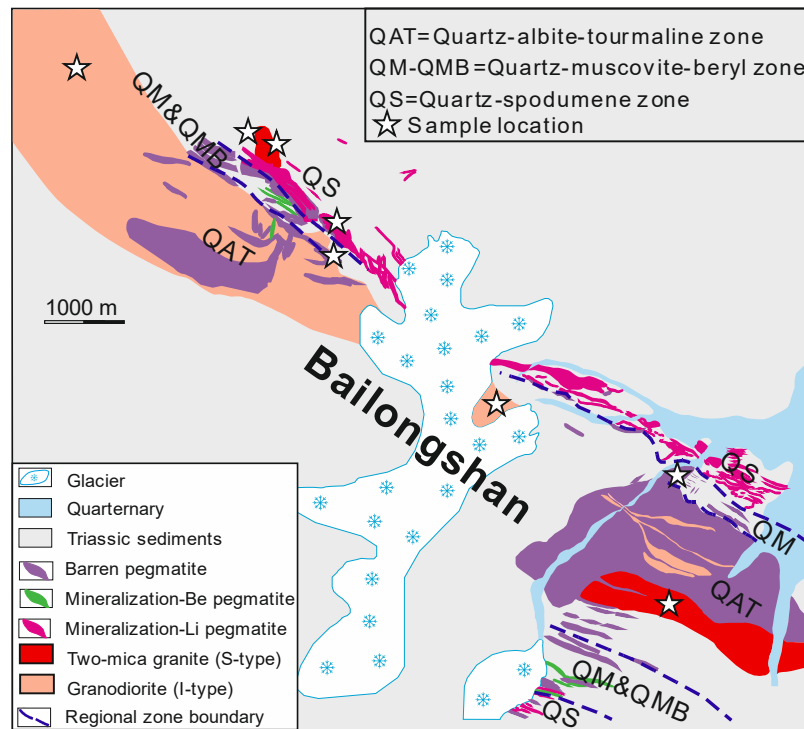


**Figure S1.** Simplified geological map of the Bailongshan rare-metal pegmatite deposits in the western Kunlun, NW Tibet plateau (after Yan et al., 2022).

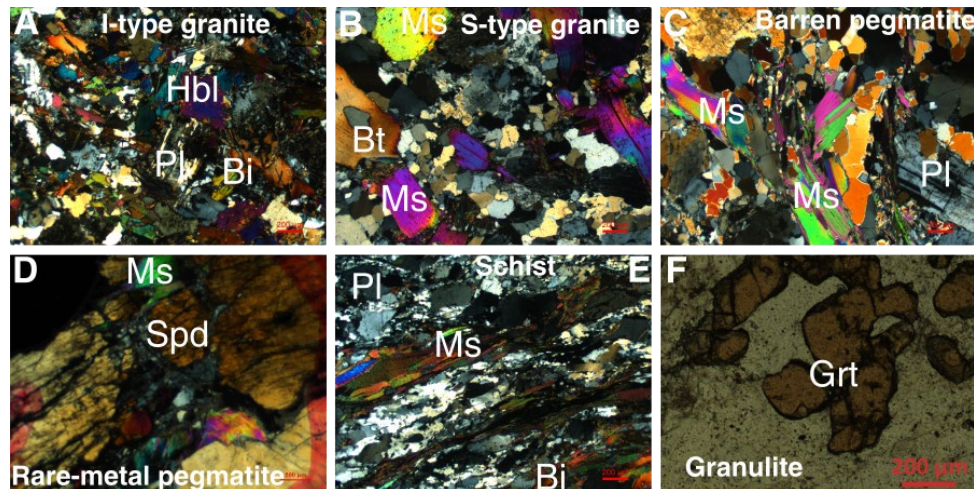
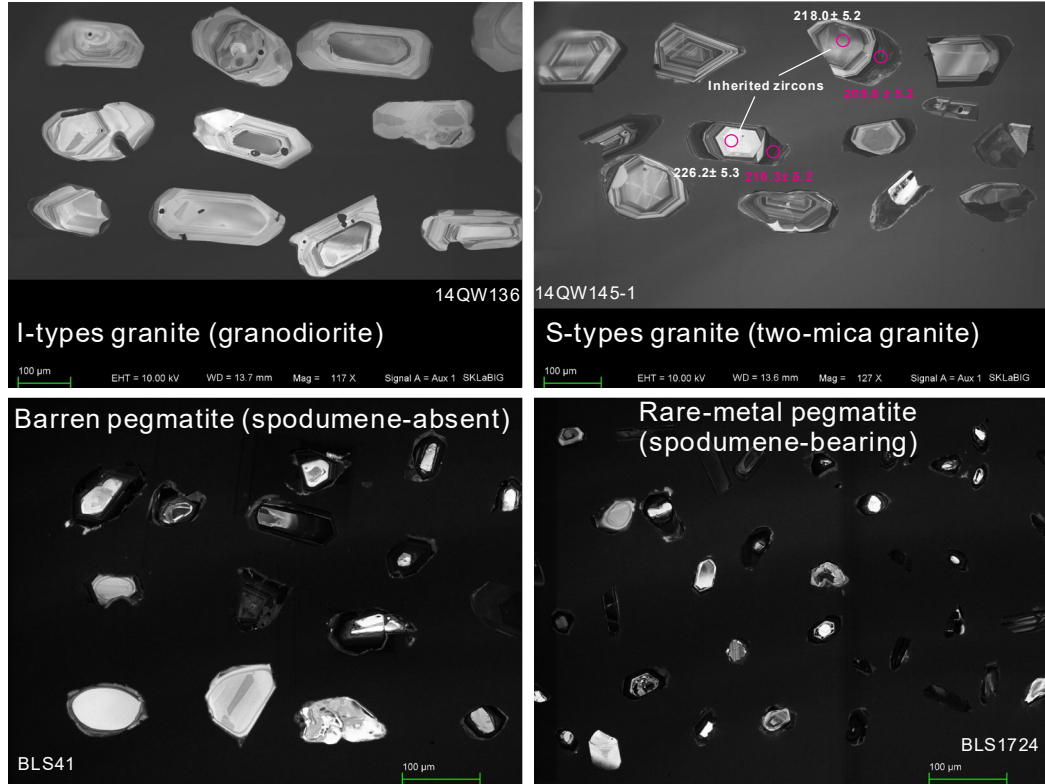


**Figure S2.** Photomicrographs of the representative samples. Hbl-hornblende, Pl-plagioclase, Bi-biotite, Ms-muscovite, Spd-spodumene, Grt-garnet.



A



B

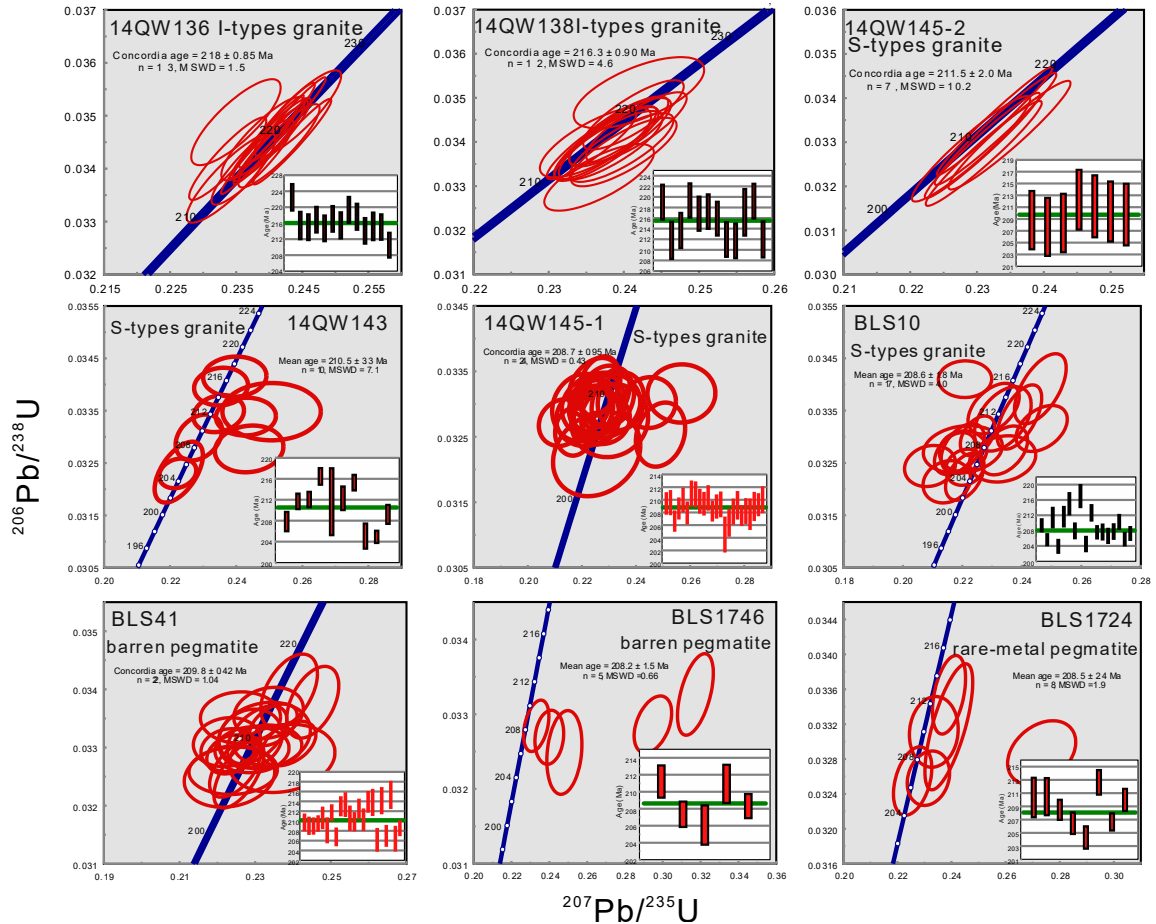


**Figure S3.** (A) Cathodoluminescence (CL) images of representative zircon grains, showing the inherited zircons generally occurred as grain cores that have older  $^{206}\text{Pb}/^{238}\text{U}$  ages compared to corresponding rims. (B) Concordia diagrams of zircon U-Pb dating and weighted-mean  $^{206}\text{Pb}/^{238}\text{U}$  ages distribution plots.

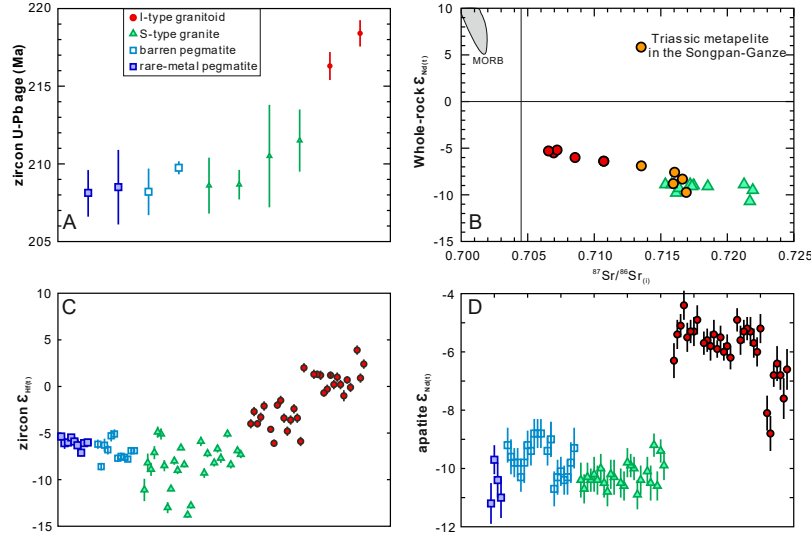


**Figure S4.** Age summary and Sr-Nd-Hf isotopes of the rocks from the Bailongshan deposit. (A) Summary of U-Pb zircon geochronology. (B) Whole-rock Sr-Nd isotopes plot for the I and S-type granitoids from the Bailongshan deposit in the western Kunlun (Table S6), Triassic metasedimentary rocks (metapelite) from the Songpan-Ganze (Zhao et al., 2021) are showing for comparison. The S-type granitoids show similar Sr-Nd isotopes with Triassic metapelites. (C-D) zircon Hf and apatite Nd isotopes.

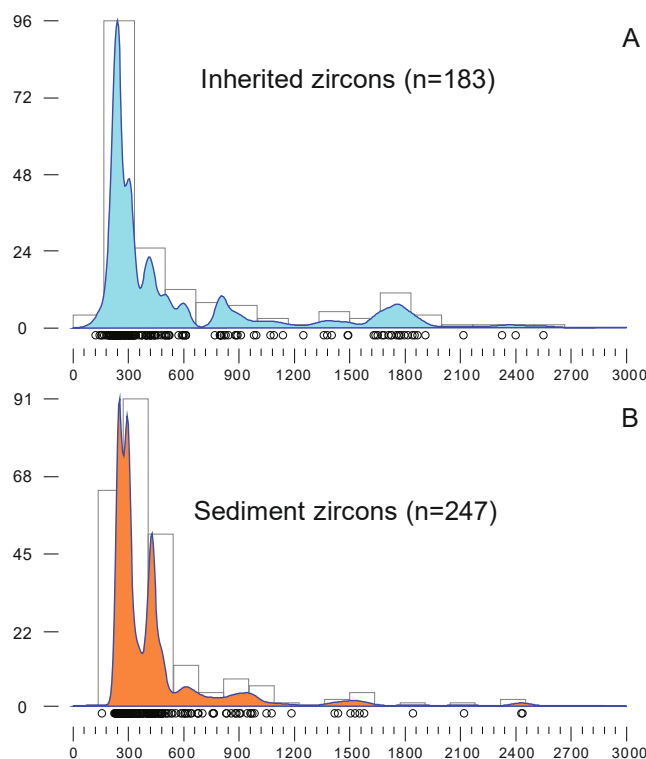


**Figure S5.** (A) Frequency histogram of inherited zircons from S-type granites and pegmatites in the Bailongshan deposit ([Table S9](#)). (B) Frequency histogram of zircons from the Triassic sedimentary complex, data source is from [Dong et al. \(2019\)](#). The inherited zircons and zircons from the Triassic sedimentary rocks show similar age spectrum, indicating that the S-type granites are derived from melting of Triassic sedimentary rocks.

## Supplementary References

- Hu, Z., Zhang, W., Liu, Y., Gao, S., Li, M., Zong, K., Chen, H., and Hu, S., 2015, "Wave" Signal-Smoothing and Mercury-Removing Device for Laser Ablation Quadrupole and Multiple Collector ICPMS Analysis: Application to Lead Isotope Analysis: *Analytical Chemistry*, v. 87, no. 2, p. 1152-1157.
- Jackson, S. E., Pearson, N. J., Griffin, W. L., and Belousova, E. A., 2004, The application of laser ablation-inductively coupled plasma-mass spectrometry to in situ U-Pb zircon geochronology: *Chemical Geology*, v. 211, no. 1-2, p. 47-69.
- Jochum, K. P., Weis, U., Stoll, B., Kuzmin, D., Yang, Q., Raczek, I., Jacob, D. E., Stracke, A., Birbaum, K., Frick, D. A., Günther, D., and Enzweiler, J., 2011, Determination of Reference Values for NIST SRM 610-617 Glasses Following ISO Guidelines: *Geostandards and Geoanalytical Research*, v. 35, no. 4, p. 397-429.

- Li, Q.-L., Li, X.-H., Liu, Y., Tang, G.-Q., Yang, J.-H., and Zhu, W.-G., 2010, Precise U-Pb and Pb-Pb dating of Phanerozoic baddeleyite by SIMS with oxygen flooding technique: *Journal of Analytical Atomic Spectrometry*, v. 25, no. 7, p. 1107-1113.
- Li, X.-H., Li, Z.-X., Sinclair, J. A., Li, W.-X., and Carter, G., 2006, Revisiting the “Yanbian Terrane”: Implications for Neoproterozoic tectonic evolution of the western Yangtze Block, South China: *Precambrian Research*, v. 151, no. 1, p. 14-30.
- Li, X.-H., Tang, G. Q., Gong, B., Yang, Y. H., Hou, K. J., Hu, Z. C., Li, Q. L., Liu, Y., and Li, W. X., 2013, Qinghu zircon: A working reference for microbeam analysis of U-Pb age and Hf and O isotopes: *Chinese Science Bulletin*, v. 58, no. 36, p. 4647-4654.
- Liu, Y. S., Gao, S., Hu, Z. C., Gao, C. G., Zong, K. Q., and Wang, D. B., 2010, Continental and Oceanic Crust Recycling-induced Melt-Peridotite Interactions in the Trans-North China Orogen: U-Pb Dating, Hf Isotopes and Trace Elements in Zircons from Mantle Xenoliths: *Journal of Petrology*, v. 51, no. 1-2, p. 537-571.
- Liu, Y. S., Hu, Z. C., Gao, S., Güntherr, D., Xu, J., Gao, C. G., and Chen, H. H., 2008, In situ analysis of major and trace elements of anhydrous minerals by LA-ICP-MS without applying an internal standard: *Chemical Geology*, v. 257, no. 1-2, p. 34-43.
- Ludwig, K. R., 2003, User's manual for Isoplot 3.00: a geochronological toolkit for Microsoft Excel: Berkeley Geochronology Center Special Publication, v. 4, p. 1-70.
- Morel, M. L. A., Nebel, O., Nebel-Jacobsen, Y. J., Miller, J. S., and Vroon, P. Z., 2008, Hafnium isotope characterization of the GJ-1 zircon reference material by solution and laser-ablation MC-ICPMS: *Chemical Geology*, v. 255, no. 1, p. 231-235.
- Sláma, J., Košler, J., Condon, D. J., Crowley, J. L., Gerdes, A., Hanchar, J. M., Horstwood, M. S. A., Morris, G. A., Nasdala, L., Norberg, N., Schaltegger, U., Schoene, B., Tubrett, M. N., and Whitehouse, M. J., 2008, Plešovice zircon — A new natural reference material for U-Pb and Hf isotopic microanalysis: *Chemical Geology*, v. 249, no. 1, p. 1-35.
- Whitehouse, M. J., Claesson, S., Sunde, T., and Vestin, J., 1997, Ion microprobe U-Pb zircon geochronology and correlation of Archaean gneisses from the Lewisian Complex of Gruinard Bay, northwestern Scotland: *Geochimica et Cosmochimica Acta*, v. 61, no. 20, p. 4429-4438.
- Wiedenbeck, M., Allé, P., Corfu, F., Griffin, W., Meier, M., Oberli, F., Quadt, A. V., Roddick, J., and Spiegel, W., 1995, Three natural zircon standards for U-Th-Pb, Lu-Hf, trace element and REE analyses: *Geostandards and Geoanalytical Research*, v. 19, no. 1, p. 1-23.
- Wu, F. Y., Yang, Y. H., Xie, L. W., Yang, J. H., and Xu, P., 2006, Hf isotopic compositions of the standard zircons and baddeleyites used in U-Pb geochronology: *Chemical Geology*, v. 234, no. 1-2, p. 105-126.
- Xu, L., Hu, Z., Zhang, W., Yang, L., Liu, Y., Gao, S., Luo, T., and Hu, S., 2015, In situ Nd isotope analyses in geological materials with signal enhancement and non-linear mass dependent fractionation reduction using laser ablation MC-ICP-MS: *Journal of Analytical Atomic Spectrometry*, v. 30, no. 1, p. 232-244.
- Yan, Q.-H., Wang, H., Chi, G., Wang, Q., Hu, H., Zhou, K., and Zhang, X.-Y., 2022, Recognition of a 600-km-long Late Triassic rare-metal (Li-Rb-Be-Nb-Ta)

- pegmatite belt in the Western Kunlun orogenic belt, western China: *Economic Geology*, v. 117, no. 1, p. 213-236.
- Zhang, W., Hu, Z., and Liu, Y., 2020, Iso-Compass: new freeware software for isotopic data reduction of LA-MC-ICP-MS: *Journal of Analytical Atomic Spectrometry*, v. 35, no. 6, p. 1087-1096.
- Zhao, H., Chen, B., Huang, C., Bao, C., Yang, Q., and Cao, R., 2021, Geochemical and Sr-Nd-Li isotopic constraints on the genesis of the Jiajika Li-rich pegmatites, eastern Tibetan Plateau: implications for Li mineralization: *Contributions to Mineralogy and Petrology*, v. 177, no. 1, p. 4.
- Zong, K., Klemm, R., Yuan, Y., He, Z., Guo, J., Shi, X., Liu, Y., Hu, Z., and Zhang, Z., 2017, The assembly of Rodinia: The correlation of early Neoproterozoic (ca. 900Ma) high-grade metamorphism and continental arc formation in the southern Beishan Orogen, southern Central Asian Orogenic Belt (CAOB): *Precambrian Research*, v. 290, p. 32-48.